Chinese Journal of Acoustics, 16(2), 1997: 121-134

An efficient absorbing boundary for finite-difference time-domain field modeling in acoustics*

WANG Shuozhong

(*Shanghai University*, Shanghai 200072)

Abstract This paper presents a highly efficient absorbing boundary condition suitable for use in the finite-difference time-domain (FDTD) modeling of acoustic fields. The new method seeks a least square estimate of a transfer matrix for field components near truncating boundaries by means of matrix pseudo-inversion. The proposed absorbing boundary is considerably more effective than a number of existing ones. The method is also computationally economical and robust. The performance of the new method is demonstrated by numerical experiments on a point-source radiation problem, a wedge diffraction problem, and a scattering problem in which a plane wave is scattered by a circular cylinder.

I. Introduction

The finite-difference time-domain (FDTD) method widely used in the numerical computation of electromagnetic fields was initially proposed by Yee[1]. This method gives the field solutions by using a set of difference equations in place of the Maxwell担 equations, and simulating the propagation of the waves in the time domain in a recursive fashion. The success of the FDTD lies in the fact that the Maxwell担 curl equations can be represented by a set of explicit recursive relations. The algorithm is simple and robust; and the boundary conditions are satisfied naturally in the process of the recursion.

In acoustics, a finite difference method was used to solve the Helmholtz integral equation in order to calculate the radiated sound distribution from measurements around an underwater structure[2]. Fricke used a Lax-Wendroff conservation law finite-difference scheme to discretize a set of elastodynamic equations in his studies of sound scattering from Arctic ice features[3]. Applications of finite difference methods based on discretization of the wave equation within elastic bodies to the studies of seismic waves in seafloor environments were reviewed by Stephen[4].

A set of FDTD recurrence formulae for linear acoustics can also be obtained directly from Euler担 equation and the equation of continuity. This is achieved by replacing the first-order derivatives with respect to spatial and temporal coordinates respectively by relevant central differences[5]. These formulae can be used to simulate sound wave propagation in the time domain to give accurate field distributions, so that some problems that are difficult to deal with using other methods may be solved. The FDTD method is expected to be useful in aspects of acoustics such as scattering of sonar targets, radiation properties of transducers, etc.

* This work is supported by the National Natural Science Foundation of China.

In any FDTD field modeling, computation must be confined to a bounded space due to limited computer resources. The field is truncated on an outer boundary that encloses all scatterers. The boundary is said to be ideally absorbing if all waves are out-going without non-physical reflection from it back to the region. An accurate field distribution may be obtained inside ideally absorbing boundaries as if there were no truncation. This is equivalent to moving the radiation condition at infinity[6] to the finitely located truncating boundary. Clearly, any non-physical reflection will result in artifacts and excessive errors in the obtained field data. Therefore the absorbing boundary condition (ABC) has been a research topic attracting much attention. Yee did not use any ABC when he first proposed the FDTD method, but simply set the field on truncating boundaries to zero. Later, many different techniques of boundary treatment emerged in order to improve the FDTD performance. An early method was used by Taflove et al.[7] termed the out-going wave averaging ABC. Mur[8] introduced a popular ABC, which may take the forms of the first or high orders according to different requirements of accuracy. A 捞uperabsorption" technique has been proposed by Mei et al.[9], based upon analyses of residual reflections caused by the use of an ABC. This technique effectively reduces non-physical reflections from the boundary as it is essentially a second-order method when used in conjunction with a first-order ABC. In acoustics, Keys[10] suggested a second order ABC, obtained by decomposing the scalar wave equation into an out-going and an in-coming component. Railton et al.[11] have made comparisons of several ABCs, including the first-order Mur担 and some second-order methods, and in particular, the superabsorption. Although the performances of these second-order methods vary in different situations, they are generally considered as being in the same range.

This paper presents a different method for treating absorbing boundaries. The new method uses a least square estimation to derive the relation between adjacent lattice lines inside the truncating boundary. The field values on the entire boundary are obtained concurrently through matrix algebraic operations. Section II discusses the principle, and describes the numerical method. Section III deals with some underwater acoustic problems using the FDTD algorithm with the proposed ABC. Comparisons are made between the proposed ABC and some widely used ones, including the superabsorption representing second-order methods. It is shown that the performance of the proposed ABC is superior to that of the others. The new ABC is also simple in form, and computationally efficient. The final section concludes the paper. The discussion is confined to 2-D cases for simplicity. Generalization to 3-D should be straightforward.

II. Principles and numerical methods

1. *FDTD Formulae and Absorbing Boundary Conditions*

Consider sound waves propagating in the water. Define a computation domain sized $L_x \times L_y$ in which FDTD recurrences are carried out. Since one of our goals is to study scattering from objects with a finite acoustic impedance, and both sound pressure and particle velocity are likely to appear in the expressions of the boundary condition on the object surface, a non-staggered lattice is chosen. Nevertheless, a staggered lattice structure may be appropriate in different applications. The method discussed here is applicable to both lattice structures. Assume that a plane wave enters the computation domain from the left, and all scatterers are inside the domain. In a 2D Cartesian coordinate system, the sound pressure, p, and the particle velocity, $\mathbf{u}$, are obtained from the following recurrence expressions[5]:

$$u_x^{(n)}(i,j) = u_x^{(n-2)}(i,j) - \frac{\Delta t}{\delta\rho}\left[p^{(n-1)}(i+1,j) - p^{(n-1)}(i-1,j)\right], \quad (1)$$

$$u_y^{(n)}(i,j) = u_y^{(n-2)}(i,j) - \frac{\Delta t}{\delta\rho}\left[p^{(n-1)}(i,j+1) - p^{(n-1)}(i,j-1)\right], \quad (2)$$

$$p^{(n)}(i,j) = p^{(n-2)}(i,j) - \frac{\rho c^2 \Delta t}{\delta}\left[u_x^{(n-1)}(i+1,j) - u_x^{(n-1)}(i-1,j) + u_y^{(n-1)}(i,j+1) - u_y^{(n-1)}(i,j-1)\right]. \quad (3)$$

In these expressions, i and j are spatial indices; and n is a temporal index. ρ is the density of the medium (water), and c the sound speed. δ is the lattice spacing, which should be small enough, normally one tenth of the wavelength or less, to provide an adequate accuracy. The time step must satisfy the inequality, $\Delta t < \delta/(\sqrt{2}c)$, to ensure stability of the algorithm. The total numbers of lattice nodes in both directions are $N_x=L_x/\delta+1$ and $N_y=L_y/\delta+1$, respectively.

Based on Equations (1)–(3), the present sound pressure at any lattice node is obtained from the pressure at the same node two time-steps earlier, together with the particle velocities of the previous time step at its four surrounding nodes. The particle velocity is computed in a similar way. A computer program can be written to update **u** and p alternately without solving any system of simultaneous equations.

In the usual treatment of the absorbing boundary, expressions for evaluating the boundary points may be established based on the relations between the field values on the boundary and on the adjacent lattice lines inside the boundary, and between the current and previous time-steps. For example, the field value of a boundary point on the boundary line $i=N_x$ can be approximated by the average of the values at the three nearest nodes on the adjacent lattice line $i=N_x-1$ and at the previous time-step[7]:

$$f^{(n)}(N_x, j) = \frac{1}{3}\left[f^{(n-2)}(N_x-1, j-1) + f^{(n-2)}(N_x-1, j) + f^{(n-2)}(N_x-1, j+1)\right], \quad (4)$$

where f may be any field component, and $\Delta t=\delta/2c$ is assumed. This method may be termed the out-going wave averaging ABC. Our experiments have shown that the method can be modified by estimating the wave propagation direction near the truncating boundary, resulting in an improved weighted averaging ABC:

$$f^{(n)}(N_x, j) = \xi f^{(n-2)}(N_x-1, j-1) + \eta f^{(n-2)}(N_x-1, j) + \zeta f^{(n-2)}(N_x-1, j+1), \quad (5)$$

where the weighting coefficients ξ, η, and ζ are the functions of α, which is the angle between the direction of the wave propagation and the x-axis:

$$\xi = \frac{1}{2}\tan\alpha\,(1+\tan\alpha), \quad \eta = (1+\tan\alpha)(1-\tan\alpha), \quad \zeta = -\frac{1}{2}\tan\alpha\,(1-\tan\alpha). \quad (6)$$

Alternatively, the popular Mur担 first order ABC[8] is:

$$f^{(n)}(N_x, j) = f^{(n-1)}(N_x-1, j) + \frac{c\Delta t-\delta}{c\Delta t+\delta}\left[f^{(n)}(N_x-1, j) - f^{(n-1)}(N_x, j)\right]. \quad (7)$$

In this expression, the direction of the out-going waves is assumed to be perpendicular to the truncating boundary. The Mur担 higher order ABCs with improved performances can be obtained by the inclusion of the higher-order terms when considering the wave propagation properties. The higher-order ABCs usually

have more involved forms, especially in the case of a non-staggered lattice structure. The improvements that the second-order Mur担 ABC offers appear to be insignificant in our experiments.

Using the superabsorption technique in conjunction with several first-order ABCs, the weighted averaging method in particular, has to various extents enhanced the absorbing capability of the truncating boundary. Some of the numerical results will be presented in Section III.

2. *Least Square Absorbing Boundary Condition*

In the ABCs described above, calculations of the boundary values are carried out point by point during the FDTD recurrence, based on certain spatial and temporal relations of the field values. A different approach is adopted in the present work. Consider the boundary $i=N_x$, $j=1,2,...,N_y$. In the vicinity of an ideally absorbing boundary, waves should travel outward without reflection. Therefore each boundary value may be obtained from a linear combination of the values on the lattice line immediately inside the boundary, $i=N_x-1$, $j=1,2,...,N_y$:

$$f^{(n)}(N_x, j) = \sum_{l=1}^{N_y} h_{jl} f^{(n-2)}(N_x - 1, l) \ , \qquad j=1,2,...,N_y \ . \tag{8}$$

Expressed in terms of matrix algebra, the field distributions on the lines $i=N_x$ and $i=N_x-1$, and at successive recurrence steps may be related through an $N_y \times N_y$ matrix, **H**:

$$\mathbf{f}_{00} = \mathbf{H}\ \mathbf{f}_{11} \ . \tag{9}$$

The $N_y \times 1$ vector $\mathbf{f}_{00}$ represents all the current field values on the entire boundary $i=N_x$, where the first "0" in the subscript indicates the current time instant as denoted by (n) in the superscripts of the FDTD formulae, while the second "0" indicates that the distance from the boundary is zero. In the subscript of the $N_y \times 1$ vector, $\mathbf{f}_{11}$, on the right side of the equation, the first "1" indicates the previous time-step, namely the time instant ($n-2$), while the second "1" indicates that the distance from the boundary is 1δ. Similarly, the field values two time-steps earlier on the lines $i=N_x-2$ (2δ from the boundary) and $i=N_x-3$ (3δ from the boundary) should be denoted as $\mathbf{f}_{22}$ and $\mathbf{f}_{23}$, respectively. With this notation, the ABCs for the four boundaries of the rectangular region will take the same form. **H** may be termed the transfer matrix. It is clear that the boundary values $\mathbf{f}_{00}$ can be obtained from $\mathbf{f}_{11}$ if **H** is known.

A similar relation exists between $\mathbf{f}_{11}$ and $\mathbf{f}_{22}$:

$$\mathbf{f}_{11} = \mathbf{H}_1 \mathbf{f}_{22} \ . \tag{10}$$

Here $\mathbf{f}_{11}$ and $\mathbf{f}_{22}$ are available as they were computed in the previous FDTD recurrences, and stored. For $\mathbf{H}_1$, Equation (10) is a system of underdetermined linear equations with N_y equations and N_y^2 unknowns, therefore has an infinite number of solution sets. A solution in the least square (LS) sense can be obtained using the {1,3}-generalized inverse of $\mathbf{f}_{22}$, or the LS pseudo-inverse, $\mathbf{f}_{22l}^{-}$ [12]:

$$\mathbf{H}_1 = \mathbf{f}_{11}\mathbf{f}_{22l}^{-} \ . \tag{11}$$

Normally, the {1,3}-generalized inverse is not unique. Since the rank of $\mathbf{f}_{22}$ is equal to its column number, nevertheless, the {1,3}-generalized inverse happens to be the {1,2,3,4}-generalized inverse, or Moore-Penrose pseudo-inverse, $\mathbf{f}_{22}^{+}$, which is indeed unique. Thus

$$\mathbf{H}_1 = \mathbf{f}_{11}\mathbf{f}_{22}^{+} \ . \tag{12}$$

The Moore-Penrose pseudo-inverse of an $M\times N$ matrix, $\mathbf{F}$, may be obtained by means of singular value decomposition (SVD). The SVD of $\mathbf{F}$ is

$$\mathbf{F} = \mathbf{U}\boldsymbol{\Lambda}\mathbf{V}^* , \tag{13}$$

where $\mathbf{U}$ is an $M\times M$ matrix with its columns being the eigenvectors of $\mathbf{F}\mathbf{F}^*$; and $\mathbf{V}$ is an $N\times N$ matrix with its columns being the eigenvectors of $\mathbf{F}^*\mathbf{F}$. $\mathbf{F}^*$ is the complex conjugate of $\mathbf{F}$. $\boldsymbol{\Lambda}$ is an $M\times N$ matrix whose "diagonal" elements, $\lambda_{ii} = \lambda_i$ (i = 1, 2, ..., rank($\mathbf{F}$)), are the singular values of $\mathbf{F}$, and other elements are all zero. λ_i^2s are the non-zero eigenvalues of $\mathbf{F}\mathbf{F}^*$ and $\mathbf{F}^*\mathbf{F}$. The pseudo-inverse of $\mathbf{F}$ can be calculated by

$$\mathbf{F}^+ = \mathbf{V}\boldsymbol{\Lambda}^+\mathbf{U}^* . \tag{14}$$

The pseudo-inverse of $\boldsymbol{\Lambda}$ in this equation can easily be obtained by taking its transpose and replacing the non-zero diagonal elements with their reciprocals. It is therefore clear that the pseudo-inversion problem may be solved by solving a relevant eigenvalue problem.

In a 2D case where N=1, $\mathbf{F}$ degenerates to a column vector $\mathbf{f}$. Since the rank of $\mathbf{f}$ is 1, only one non-zero element λ_1 exists in $\boldsymbol{\Lambda}$, and $\mathbf{V}$ becomes a scalar 1. The eigenvalue λ_1 and the corresponding eigenvector $\mathbf{u}_1$ can be obtained by an iterative method that converges quickly. Thus the pseudo-inverse of $\mathbf{f}$ is computed:

$$\mathbf{f}^+ = \frac{1}{\lambda_1}\mathbf{u}_1^* . \tag{15}$$

Since the least square solution of the underdetermined system of equations, $\mathbf{H}_1$, is rigorous, $\|\mathbf{f}_{11}-\mathbf{H}_1\mathbf{f}_{22}\|$ should be within the range of the computer round-off errors.

The field property usually does not change appreciably in a range as small as a fraction of one wavelength. Therefore the solution $\mathbf{H}_1$ obtained from Equation (12) may be used as an estimate of $\mathbf{H}$ in Equation (9). This yields a simple expression for estimating $\mathbf{f}_{00}$ from $\mathbf{f}_{22}$ and $\mathbf{f}_{11}$:

$$\hat{\mathbf{f}}_{00} = \mathbf{H}_1\,\mathbf{f}_{11} = \mathbf{f}_{11}\,\mathbf{f}_{22}^+\,\mathbf{f}_{11} . \tag{16}$$

From Equation (16) we can see that, in each recurrence step, the boundary values are updated through matrix pseudo-inversion and multiplication. As the least-square solution of the transfer matrix $\mathbf{H}$ has been used, the new absorbing boundary condition will be referred to as the least-square (LS) ABC in this paper for the sake of convenience.

Due to the discrete nature of the FDTD method, however, $\mathbf{f}_{11}$ and $\mathbf{f}_{22}$ contain numerical noise that causes intolerable errors, making the expression (16) practically unusable. This noise can be significantly reduced by a smoothing operation in each recurrence step. A simple averaging method is recommended for this purpose:

$$\bar{\mathbf{f}}_{11} = \left[\mathbf{f}_{12} + w\,\mathbf{f}_{11} + \mathbf{f}_{10}\right]/(2+w) , \tag{17}$$

$$\bar{\mathbf{f}}_{22} = \left[\mathbf{f}_{23} + w\,\mathbf{f}_{22} + \mathbf{f}_{21}\right]/(2+w) . \tag{18}$$

Replace $\mathbf{f}_{11}$ and $\mathbf{f}_{22}$ with $\bar{\mathbf{f}}_{11}$ and $\bar{\mathbf{f}}_{22}$, respectively, in Equation (16):

$$\hat{\mathbf{f}}_{00} = \bar{\mathbf{f}}_{11}\bar{\mathbf{f}}_{22}^+\bar{\mathbf{f}}_{11} . \tag{19}$$

Equations (17)–(19) form the basic expressions of the LS ABC. They are independent of any field parameters and the lattice structure, lattice spacing, time step, etc. The parameter w in Equations (17) and (18) is a complex weighting coefficient that can be adjusted through experiments to obtain a near optimal result.

Numerical Experiments show that the algorithm is stable as w varies within a small area around unit in the complex plane.

The parameter E defined in the following may be used as a measure of the error in the field value estimate on the truncating boundary:

$$E = \frac{(\hat{\mathbf{f}}_{00} - \mathbf{f}_{00})^* \ (\hat{\mathbf{f}}_{00} - \mathbf{f}_{00})}{\mathbf{f}_{00}^* \mathbf{f}_{00}} = \frac{\mathbf{f}_{11}^* (\mathbf{H}_1 - \mathbf{H})^* \ (\mathbf{H}_1 - \mathbf{H}) \mathbf{f}_{11}}{\mathbf{f}_{00}^* \mathbf{f}_{00}} \quad . \tag{20}$$

It is clear that the error mainly results from the difference between $\mathbf{H}_1$ and $\mathbf{H}$. An example showing the magnitude of this error will be given in the numerical computation presented in the next section.

III. Numerical computations

To show the performance of the LS ABC, FDTD computations for some acoustic field problems are carried out in a Cartesian coordinate system. These problems include radiation of a point source, diffraction by a wedge, and scattering from a cylinder. The computation domain is $1 \le i \le N_x$, $1 \le j \le N_y$. In the point-source-radiation and cylinder-scattering problems, the LS method will be compared with other methods quantitatively in terms of the residual non-physical reflection from the boundary. In the wedge-diffraction and cylinder-scattering problems, the effects of different ABCs upon the diffracted field and the far-field directional patterns of the scattered waves will be studied. These will show the usefulness of the proposed ABC in practical applications.

1. *Radiation of a Point Source*

Let a point source be located at the bottom-left corner of the computation domain (i=1, j=1). It starts a harmonic oscillation, and the adjacent particles all move in radial directions. As the FDTD recurrence proceeds, the disturbance spreads out cylindrically, and then encounters the truncating boundary at $i=N_x$, and $j=N_y$. In order to study the absorbing boundary performance, the FDTD algorithm is first applied to an area larger than the computation domain, as shown in Figure 1. Let the FDTD recurrence terminate before the wave front reaches the larger area担 outer boundary. If the area is large enough, a steady-state field without the influence of the outer boundary is established in the computation domain by this time. The sound pressure distribution in the computation domain is stored, and will be used as the reference for the evaluation of the ABC performances. The FDTD recurrence is then confined to the computation domain, using the same initial condition and the same number of recurrence steps as in the generation of the reference to ensure an identical phase. Several ABCs are used at the truncating boundaries. The residual non-physical reflection is obtained by subtracting the resultant pressure distribution from the reference.

The size of the computation domain in Figure 1 is 4m×4m. The FDTD parameters used are: $L=\lambda/\delta$=12, $\Delta t=\delta/2c$, therefore $N_x=N_y$=49. The recurrence-step number used in the computation is 69. The instantaneous pressure distribution is visualized by the gray level map in the plot, with the intermediate gray shade representing zero, and the darker and brighter shades representing negative and positive excursions respectively. The point source is modeled by

$$p^{(n)}(1,1) = \exp(-j\omega n\Delta t), \tag{21}$$

and p, u_x and u_y at the three points (1,2), (2,1) and (2,2) are oscillating at the same frequency and each with an appropriate amplitude and phase. This source model is not isotropic in a Cartesian system. Nevertheless it does not affect the validity of our discussion.

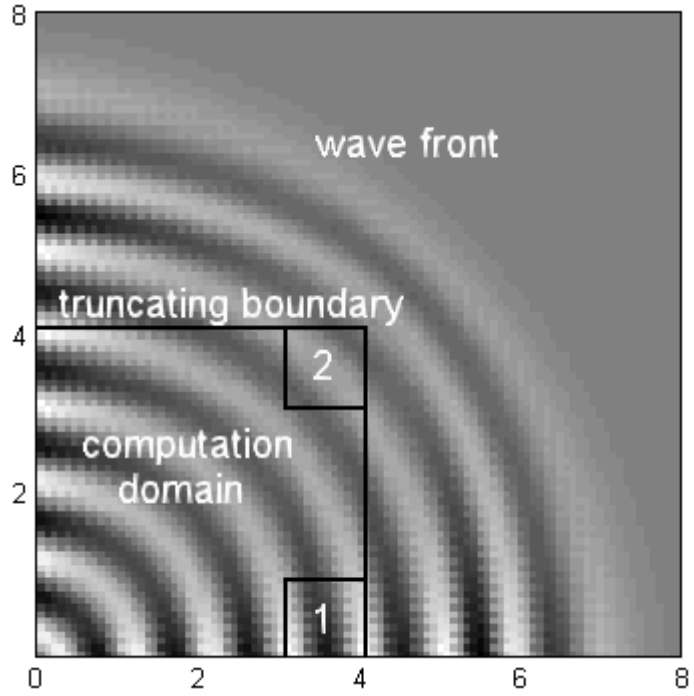

Figure 1 Study ABC performance through radiation of a point source. The unit is meter.

In order to describe the ABC performance quantitatively, a boundary reflectivity is defined. Take two squares, S_1 and S_2, with their sides equal to one wavelength, as shown in Figure 1. The following parameter may be used as a measure of the boundary-generated residual non-physical reflection:

$$R_k = \frac{\sum_{i,j \in \mathbf{S}_k} \left| p_d(i,j) - p_r(i,j) \right|^2}{\sum_{i,j \in \mathbf{S}_k} \left| p_r(i,j) \right|^2}, \qquad \text{k=1, 2.} \tag{22}$$

In this equation, p_d is obtained from the FDTD recurrence, while p_r is the reference pressure. R_1 may be considered as the reflectivity of the boundary under normal incidence, whereas R_2 is associated with oblique incidence. The latter includes contributions from both the right and the upper boundaries.

For a non-staggered lattice structure, both p and **u** on the boundary must be evaluated. Since the LS method is concise and fast, this poses little burden on the FDTD algorithm. With some other ABCs such as the second order Mur扭, however, the need for evaluating both p and **u** may result in a lengthy program and require considerably more computer time.

The values of boundary reflectivity in the point-source radiation experiment, calculated from Equation (22), are listed in Table 1. In addition to the proposed LS ABC, the first order Mur扭 ABC, the simple out-going wave averaging ABC, and the weighted averaging ABC are tested for comparison. The latter three methods are also used in conjunction with the superabsorption technique. It is observed from the table that the LS ABC produces the least unwanted reflection among all the methods in both normal and oblique incidence cases. In particular, the non-physical reflection of the LS ABC is considerably less than that

produced by the weighted averaging method with a superabsorption procedure, whereas the computer program of the LS ABC is much more concise than that of the superabsorption procedure.

Table 1 also gives the total computation time of the algorithm (that is, FDTD recurrence inside the computation domain plus calculation of the ABC), t_{total}, and the time consumed solely by the ABC, t_{ABC}, in each case. The numerical experiments were carried out on a 486DX2-66 computer. The time consumed by the LS ABC calculation is on the same order as that by the first order Mur担 and the simple out-going wave averaging ABCs. It is much less than the time taken by the weighted averaging and the superabsorption procedure. Note that the consumed time by the LS ABC is only a fraction of the total in this experiment. When there exist scatterers, this proportion can be even lower.

Table 1 Comparison of performances of different ABCs in the point source radiation problem.

Absorbing Boundary Condition	R_1	R_2	t_{total} (s)	t_{ABC} (s)
First Order Mur	0.2343	0.1121	113.2	5.1
First Order Mur + Super"	0.1084	0.0678	122.4	14.3
Out-Going Wave Averaging	0.4251	0.1841	112.6	4.5
Out-Going Averaging + Super"	0.1303	0.0440	121.8	13.7
Weighted Averaging	0.3003	0.1586	193.3	85.2
Weighted Averaging + Super"	0.0458	0.0403	207.1	99.0
Least Square (LS)*	0.0188	0.0143	113.7	5.6

* The weighting $w = 0.98 \exp(-j\pi/64)$ was used in the LS ABC.

Equation (20) has been used to calculate the errors in the sound-pressure estimate on the boundary $i=N_x$. In the calculation, $\mathbf{p}_{11}$ and $\mathbf{p}_{22}$ obtained in the FDTD recurrence are substituted for $\mathbf{f}_{11}$ and $\mathbf{f}_{22}$ in the equation, respectively. The pressure at $i=N_x$ in the reference field is used as $\mathbf{f}_{00}$. It is found that, after 69 recurrence steps, E=0.0132. This error is in the same order with the boundary reflectivities based on the LS ABC as listed in Table 1.

In the square-shaped computation domain shown in Figure 1, the smallest grazing angle on the truncating boundary is 45°. It is generally understood that non-physical reflection will increase as the grazing angle decreases[8]. In order to observe the performance of the LS ABC at small grazing angles, a rectangular area sized 5m×1.5m is used as the computation domain. In this case, the grazing angle around the small area S_2 is approximately 17°. With the first order Mur担 ABC, the reflectivities obtained are R_1=0.3674, and R_2=0.6677. They are significantly higher than the figures given in Table 1, and the ABC becomes virtually unusable. A similar situation arises when the out-going wave averaging method is used. With the LS ABC, on the other hand, the result is R_1=0.0123 and R_2=0.0455. They are still at an acceptable low level. Since R_1 has not increased, the increase of R_2 can be attributed to the decrease of the grazing angle. Therefore the LS ABC is also advantageous in the case of small grazing angles. This, of course, is highly desirable. In the LS method, the field value of each boundary point is derived from the values of all lattice nodes on the adjacent line inside the boundary. In this way, the out-going waves coming from all directions are taken into account,

making the method relatively insensitive to the local wave propagation direction, and overcoming the drawbacks of many other ABCs.

2. *Wedge Diffraction*

Consider the diffraction of a plane wave by a wedge. When scattering objects are present in the region, the boundary conditions satisfied by the sound wave on the object surface must be expressed in a finite-difference form suitable for recurrence. Here we only consider ideal boundaries, i.e., absolutely soft and absolutely rigid cases. The FDTD formulation of complicated boundary conditions is beyond the scope of this paper. On an ideally soft boundary, the sound pressure should be set to zero in each recurrence cycle:

$$p^{(n)}(i,j)=0 \quad . \tag{23}$$

The particle velocity, **u**, is constrained by the motion equations (1) and (2). On an ideally rigid surface, the normal component of the particle velocity must be zero. For harmonic waves this leads to the following [5]:

$$p^{(n)}(i,j)=\frac{p^{(n)}(i-1,j)\cos\alpha(i,j)+p^{(n)}(i,j-1)\sin\alpha(i,j)}{\cos\alpha(i,j)+\sin\alpha(i,j)} \quad , \tag{24}$$

assuming that (i,j) is a surface point, and $(i-1,j)$ and $(i,j-1)$ are within the water. $\alpha(i,j)$ is the angle between the surface normal and the positive x axis. One of the velocity components is then calculated from an FDTD recurrence expression (1) or (2), while the other is obtained from the normal-velocity constraint:

$$u_x^{(n)}(i,j)\cos\alpha(i,j)+u_y^{(n)}(i,j)\sin\alpha(i,j)=0 \quad . \tag{25}$$

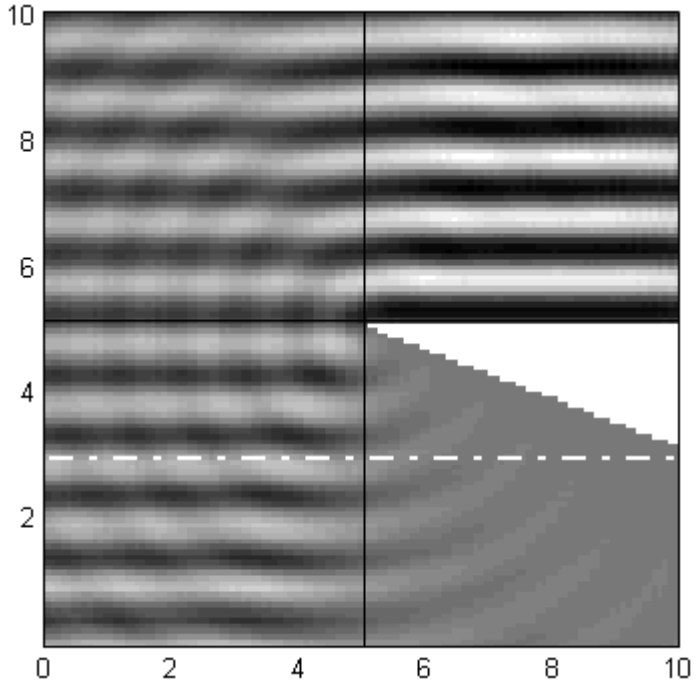

Figure 2 Diffraction of an ideally soft wedge. The vertex angle of the wedge is 21°. The wavelength of the incident sound wave is 1m. The pressure-magnitude distribution on the dash-dotted line behind the wedge and 2m from the insonified surface is illustrated in Figure 3.

Figure 2 shows an ideally soft wedge with a vertex angle of 21° with the vertex at the center of the region. The upper side is insonified perpendicularly by a plane wave with the wavelength of 1m. The computation domain is sized 10m×10m; the FDTD lattice spacing is $\delta=\lambda/12$; and the time step is $\Delta t=\delta/2c$.

Initially the top boundary is perturbed by the incidence of a plane wave, and the field inside the region is zero. The sound field distribution is obtained through FDTD recurrence, using the first Mur扭 and LS ABCs respectively. The calculated pressure distribution on the dash-dotted line behind the wedge and 2λ from the insonified face, as shown in Figure 2, is given in Figure 3.

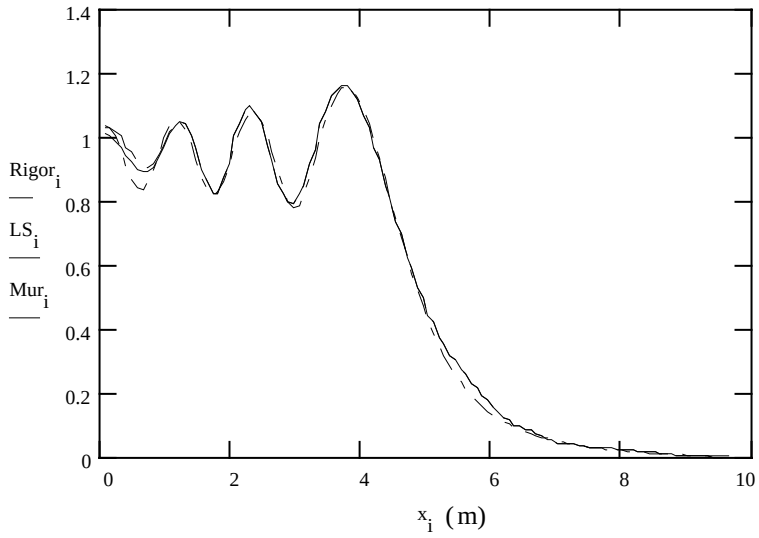

(a) After 141 recurrence steps.

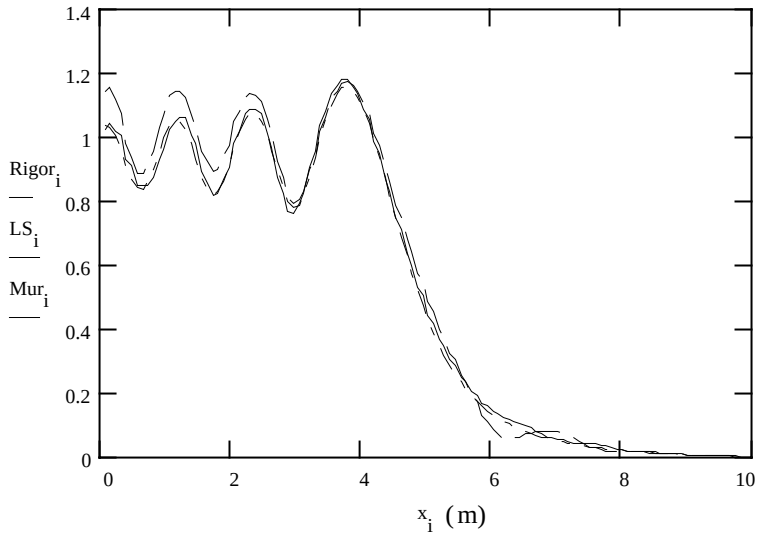

(b) After 161 recurrence steps.

Figure 3 Pressure distribution along a line behind a wedge as shown in Figure 2. The solid and dashed curves are obtained using the LS and the first order Mur's ABCs respectively. The dash-dotted curves are based on a rigorous solution.

Figure 3(a) shows the pressure distribution after 141 recurrence steps. The dotted and solid curves are obtained with the first order Mur扭 and LS ABCs, respectively. The dash-dotted curve is based on the solution in a form of an eigenfunction series using the method of separation of variables[13]. Note that at this point the diffracted wavefront has exceeded the outer boundary by about 1.6λ. The difference between the two ABCs is visible near the left boundary. Figure 3(b) shows the situation after 161 steps. By this time, the wavefront has exceeded the boundary by 3.3λ, and a steady state has been established in the computation domain. The difference between the two ABCs is substantial. The result of the LS ABC is very close to the

rigorous solution, indicating that the level of the non-physical reflection from the truncating boundary is very low. With the Mur祖 ABC, on the other hand, the errors in both the illuminated zone and the geometrical shadow are intolerably large. These errors will further increase as the FDTD recurrence proceeds.

Similar computations have been carried out for an ideally rigid wedge. The results also show that the LS method is advantagous over Mur祖 ABC.

3. *Cylinder Scattering*

Sonar target strength is an important research topic. To simulate the target scattering using the FDTD numerical procedure, the field distribution around the target can be obtained. The near-field distribution is then used to derive the far-field characteristics so that prediction of the target strength can be made. Numerical computations show that the unwanted non-physical reflection from the truncating boundary has tangible effects on the far-field characteristics. Therefore using a good ABC is a prerequisite for meaningful predictions of the target strength.

In order to observe the effect of the ABCs, consider a circular cylinder insonified by a plane wave from the left, as shown in Figure 4. Initially the left boundary of the region, i=1, is perturbed, and the field inside the region is zero. The harmonic perturbation is propagated toward the cylinder, and then scattered. The scattered wave is superimposed on the incident wave. The wave spreads out and encounters the truncating boundary in all directions. Similar to the point-source-radiation case, a larger area is used for the generation of a reference field. In order to obtain identical phases for both the field computed in the computation domain and the reference, let the left boundaries of both the computation domain and the larger area coincide.

In Figure 4 the instantaneous pressure distribution around an ideally soft cylinder with a radius a=1.6m is shown. The wavelength of the incident wave is λ=1m. The other parameters used are: $L=\lambda/\delta$=15, $\Delta t=\delta/2c$, and $N_x=N_y$=241 for the larger area sized 16m×16m. In Figure 4(a), the pressure of the total acoustic field, that is, incident plus scattered waves, around the cylinder is shown. Figure 4(b) shows the scattered wave alone, obtained by subtracting the incident plane wave from the total field. The three square areas, S_1, S_2 and S_3, with their sides equal to one wavelength are shown. In these areas the boundary reflectivities R_1, R_2 and R_3 are calculated using the same procedure as in the point-source-radiation experiment.

Table 2 Comparison of LS and Mur祖 ABCs in the cylinder scattering problem.

The Scatterer and the Absorbing Boundary Condition		Reflectivity of Total Field			Reflectivity of Scattered Wave		
		1	2	3	1	2	3
Ideally Soft	First Order Mur祖	0.4680	0.0455	0.0201	0.0252	0.2557	0.0974
	Least Square (LS)*	0.2176	0.0036	0.0022	0.0042	0.0135	0.0107
Ideally Rigid	First Order Mur祖	0.0270	0.0363	0.0116	0.0205	0.8866	0.1011
	Least Square (LS)*	0.0150	0.0087	0.0013	0.0036	0.3306	0.0110

* The weighting w = 1 was used in the LS ABC.

Table 2 gives the reflectivities obtained in the scattering experiment. A comparison of the performances of the first-order Mur祖 and the LS ABCs is made. Both soft and rigid cylinders are used. The residual non-physical reflection is calculated in S_1, S_2 and S_3. In each case, the LS ABC is superior to Mur祖 ABC.

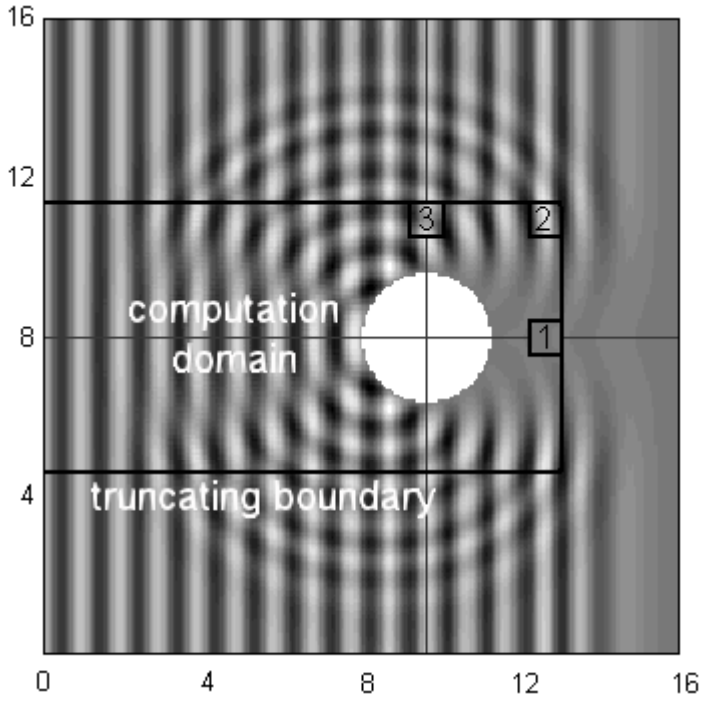

(a) Instantaneous distribution of the total acoustic pressure around the cylinder.

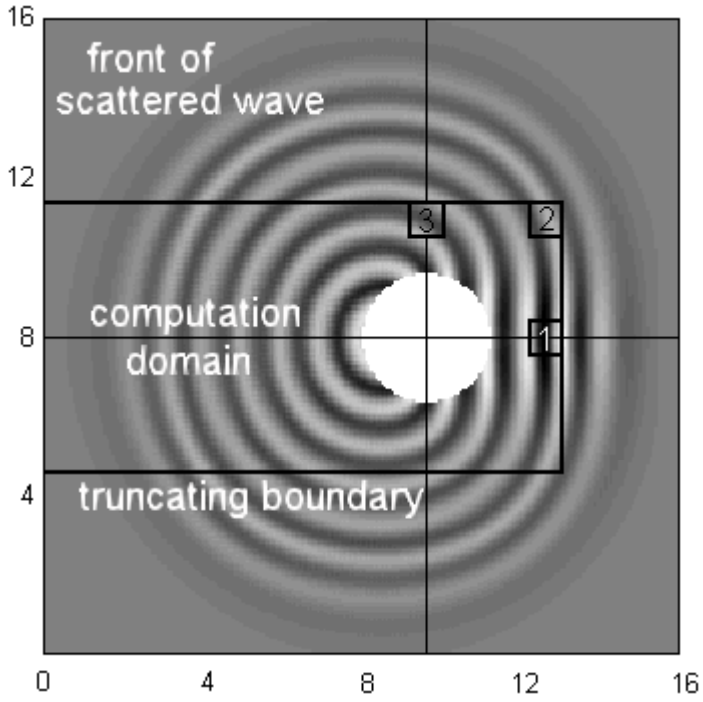

(b) Distribution of the scattered pressure.

Figure 4 Scattering of an ideally soft cylinder.

The influence of the non-physical reflection generated from the truncating boundaries is illustrated in Figure 5. In the plot, the far-field directional patterns of the scattered waves are shown. They are derived from the FDTD-calculated near field by using a discrete Fourier transform method[5,14]. Figure 5(a) presents the pressure patterns of the scattered wave from a soft cylinder. The abscissa ϕ is the directional angle. The mainlobe in the 0° direction indicates that there is strong scattering behind the object, in opposite phase with the incident wave to produce a shadow zone. The solid and dashed curves are the results of the FDTD

algorithm, with the LS (solid) and Mur扭 (dashed) ABCs, respectively. The dash-dotted curve is based on a rigorous solution in a form of a Bessel function series[15]; and the dotted curve is calculated from the reference field illustrated in Figure 4. Since the scattered wave has not reached the outer boundary of the large area as shown in Figure 4(b), this dotted curve is free of non-physical reflection from boundaries. Thus, it can be used as a reference in the comparison of different ABCs. The good agreement between the reference and the rigorous solution is an indication that the FDTD algorithm used is reliable. The solid curve is very close to the reference, while the dashed curve deviates from the reference considerably, demonstrating the superiority of the LS ABC over Mur扭.

Figure 5(b) gives the result of the ideally rigid cylinder, also showing that the LS ABC is advantageous.

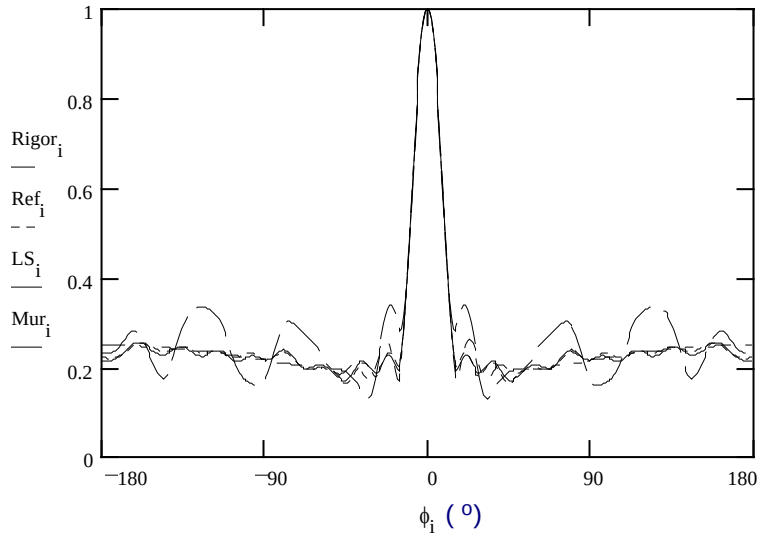

(a) Ideally soft cylinder.

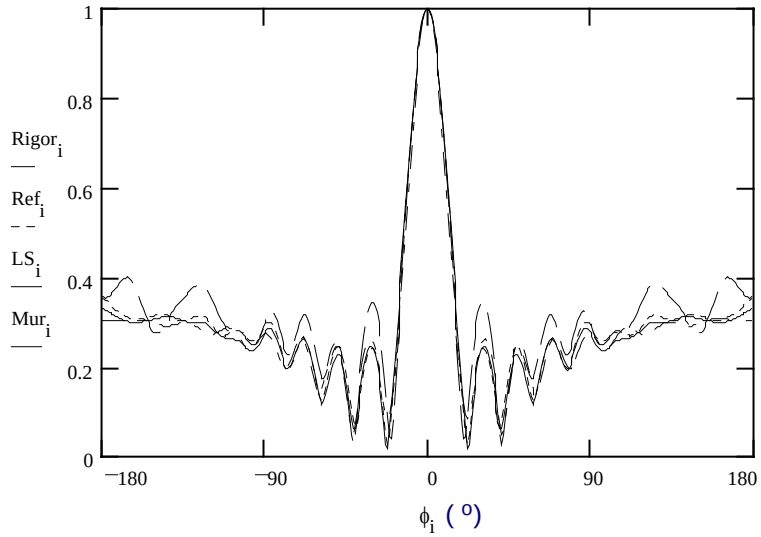

(b) Ideally rigid cylinder.

Figure 5 Influence of the residual reflection from the truncating boundary on far field directional patterns of the scattered wave from a cylinder. The solid and dashed curves are results of FDTD carried out in the computation domain, by using the LS and the first order Mur's ABCs respectively. The dotted curve is obtained from FDTD in the larger area without non-physical reflection from the outer boundary. The dash-dotted curve is a rigorous solution.

IV. Conclusions

An efficient absorbing boundary condition is a key to a successful application of the FDTD algorithm. In this paper, we have discussed the LS ABC using matrix pseudo-inversion. The proposed new ABC is efficient in the following two senses:

First, it is highly absorbent. The residual non-physical reflection generated from the outer boundary using the LS method is not only much less than that using some widely used ABCs, but also considerably less than the superabsorption result. Using the LS ABC in the target scattering applications, accurate far-field directional patterns have resulted. With the LS method, a boundary value is calculated from many internal points at more than one previous recurrence step. In the direction perpendicular to the boundary, each boundary point is related to more than one lattice line, equivalent to a higher-order treatment. In the direction parallel to the boundary, on the other hand, the matrix pseudo-inversion and multiplication operations relate each boundary point to many points on the neighboring lattice lines. This reduces the errors due to the uncertainty of the wave propagation direction.

Secondly, the LS method is computationally efficient. It takes approximately the same computer time as some of the simplest first-order methods, and is much faster than the superabsorption procedure. Besides, the LS algorithm is robust and simple in form. The field values on an entire boundary are calculated concurrently through matrix operations, making the program especially concise. For each field parameter, $\mathbf{f}$, on a boundary line, the data need to be stored in buffers are $\mathbf{f}_{11}$, $\mathbf{f}_{21}$ and $\mathbf{f}_{22}$. This takes only a fraction of the space used by the entire FDTD algorithm. More importantly, with the significantly improved ABC performance, it becomes possible to use a relatively small computation domain in the FDTD field modeling. This will substantially reduce the total computer resources required in the investigation of various field phenomena.

It is observed from expressions (17)–(19) that the only field component involved in the LS boundary evaluation is the one under consideration, independent of any other component and parameters such as ρ, c, δ and Δt. This allows a portable routine, independent of the specific problem, to be called in different applications without modification.

References

[1] K. S. Yee, 捏umerical Solution of Initial Boundary Value Problems Involving Maxwell担 Equations in Isotropic Media," *IEEE Trans. Antenna Propagat*., **AP-14** (1966), 302-307.

[2] J. A. Clark, and M. A. Sartori, "Numerical Propagation of Spatially Distributed Acoustic Sources Using the Exterior Helmholtz Integral Equation," in *IEEE Sixth SP Workshop on Statistical Signal and Array Processing Conference Proceedings*, (New York, Oct. 1992), 338-341.

[3] J. R. Fricke, 揶coustic Scattering from Elemental Arctic Ice Features: Numerical Modeling Results," *J. Acoust. Soc. Am.*, **93**(1993), 1784-1796.

[4] R. A. Stephen, 揶 Review of Finite Difference Methods for Seismo-Acoustic Problems at the Seafloor," *Rev. Geophys.*, **26**(1988), 445-458.

[5] S. Wang, 揊inite-Difference Time-Domain Approach to Underwater Acoustic Scattering Problems," *J. Acoust. Soc. Am.*, **99**(1996),1924-1931.

[6] D. Z. Wang, and E. C. Shang, 搭nderwater Acoustics," (Science Press, Beijing, 1981), 73-74. (in Chinese)

[7] A. Taflove, and M. E. Brodwin, 揑umerical Solution of Steady-State Electromagnetic Scattering Problems Using the Time-Dependent Maxwell担 Equations," *IEEE Trans. Microwave Theory Technol.*, **MTT-23** (1975), 623-630.

[8] G. Mur, 揃bsorbing Boundary Conditions for the Finite-Difference Approximation of the Time-Domain EM Field Equations," *IEEE Trans. Electromagn. Compat.*, **EMC-23** (1981), 377-382.

[9] K. K. Mei, and J. Fang, 揇uperabsorption – A Method to Improve Absorbing Boundary Conditions," *IEEE Trans. Antenna Propagat.*, **40** (1992), 1001-1010.

[10] R. G. Keys, 揃bsorbing Boundary Conditions for Acoustic Media," *Geophys.*, **50**(1985), 892-902.

[11] C. J. Railton, and E. M. Daniel, 揃 Comparison of the Properties of Radiating Boundary Conditions in the FDTD Method for Finite Discretisation and Non-Planar Waves," *IEEE Trans. Antenna Propagat.* **42**(1994), 267-281.

[12] A. Ben-Isreal, and T. N. E. Greville, *Generalized Inverse – Theory and Applications*, (John Wiley & Sons, New York, 1974), 103-121.

[13] S. Wang, 揇iffracted Acoustic Fields around a Wedge," *Chin. J. Acoust.*, **3**(1984), 121-132. (Chinese edition: *Acta Acust.*, **7**(1985), 247-256)

[14] E. V. Jull, *Aperture Antennas and Diffraction Theory*, (Perter Peregrinus, London, 1981), 38-41.

[15] P. M. Morse, *Vibration and Sound*, (American Institute of Physics, 1983), 347-350.